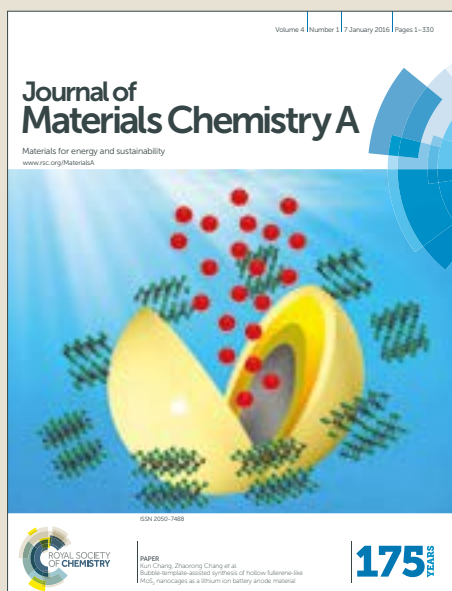


Journal of Materials Chemistry A

Accepted Manuscript



This article can be cited before page numbers have been issued, to do this please use: R. Li, G. Liu, M. Xiao, X. Yang, X. Liu, Z. Wang, L. Ying, F. Huang and Y. Cao, *J. Mater. Chem. A*, 2017, DOI: 10.1039/C7TA06631G.



This is an Accepted Manuscript, which has been through the Royal Society of Chemistry peer review process and has been accepted for publication.

Accepted Manuscripts are published online shortly after acceptance, before technical editing, formatting and proof reading. Using this free service, authors can make their results available to the community, in citable form, before we publish the edited article. We will replace this Accepted Manuscript with the edited and formatted Advance Article as soon as it is available.

You can find more information about Accepted Manuscripts in the [author guidelines](#).

Please note that technical editing may introduce minor changes to the text and/or graphics, which may alter content. The journal's standard [Terms & Conditions](#) and the ethical guidelines, outlined in our [author and reviewer resource centre](#), still apply. In no event shall the Royal Society of Chemistry be held responsible for any errors or omissions in this Accepted Manuscript or any consequences arising from the use of any information it contains.



Journal Name

ARTICLE

Non-fullerene acceptors based on fused-ring oligomers for efficient polymer solar cells *via* complementary light-absorption

Renlong Li,[‡] Gongchu Liu,[‡] Manjun Xiao, Xiye Yang, Xiang Liu, Zhenfeng Wang, Lei Ying,^{*} Fei Huang,^{*} and Yong Cao

Received 00th January 20xx,
Accepted 00th January 20xx

DOI: 10.1039/x0xx00000x

www.rsc.org/

We designed and synthesized two novel non-fullerene small molecule acceptors (IDT-N and IDT-T-N) that consist of indacenodithiophene (IDT) as the electron-donating core and the 2-(3-oxo-2,3-dihydro-1*H*-cyclopenta[*b*]naphthalen-1-ylidene)malononitrile (**N**) as a novel electron-withdrawing end group. The IDT-N and IDT-T-N consisting of the naphthyl-based (**N**) group exhibited expanded plane regarding to the phenyl-based indanone (INCN), which strengthened the intramolecular push-pull effect between the core donor unit and the terminal acceptor units. This strengthened effect resulted in a reduced bandgap that was beneficial for solar photon collection and increased short-circuit current density of the resulting devices. IDT-N and IDT-T-N exhibited red-shifted absorptions and smaller optical bandgaps than the corresponding phenyl-fused indanone end-capped chromophores. Both acceptors exhibited broad absorptions and energy levels that were well-matched with the donor materials. Polymer solar cells based on the IDT-N and IDT-T-N and two representative polymer donors (PTB7-Th and PBDB-T) exhibited impressive photovoltaic performances. The devices based on the PBDB-T:IDT-N system exhibited a power conversion efficiency of up to 9.0%, with a short-circuit current density of 15.88 mA cm⁻², and a fill factor of 71.91%. These results demonstrate that IDT-N and IDT-T-N are promising electron acceptors for use in polymer solar cells.

Introduction

Over the past two decades, polymer solar cells (PSCs) have emerged as promising candidates for solar energy collection. PSCs are typically lightweight, inexpensive, flexible, and can be fabricated using roll-to-roll coating techniques.¹⁻⁵ Fullerene and its derivatives have been widely used as acceptors in PSCs because of their high electron transport capacities, high electron affinities, and ability to form suitable forms with donor materials in bulk heterojunction (BHJ) solar cells.⁶⁻¹⁰ Power conversion efficiencies (PCEs) of greater than 11% have been achieved in devices based on fullerene derivatives, owing to the rapid development of polymeric donor materials.¹¹⁻¹⁶ However, the limitations of fullerene materials, such as the high costs of synthesis and purification, low absorption coefficients in the visible light region, and strong aggregation (resulting in poor stability), have impeded the further development of PSCs. To address these issues, polymeric and small-molecule non-fullerene acceptors (NFAs) have been incorporated into PSCs.¹⁷⁻²⁰ NFAs typically exhibit strong and broad absorption and a wide

range of energy levels and can be synthesized easily and cost-effectively.²¹⁻²⁶ Moreover, small-molecule acceptors possess well-defined molecular weights and molecular structures and can be obtained at high purities without variation between batches.²⁷⁻³⁹ By rational optimization of the electron-donating polymers and NFAs, a variety of high-performance non-fullerene PSCs have been developed with PCEs higher than 12%.^{32,40}

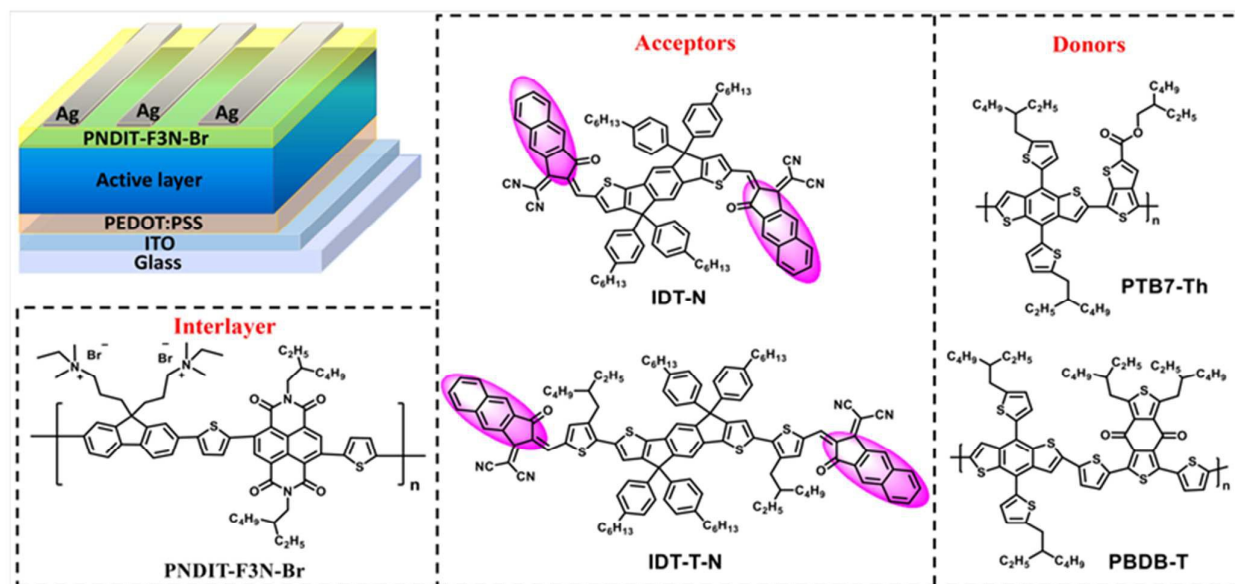
Typically, small molecular acceptors have acceptor-donor-acceptor (A-D-A)-type molecular structures. For instance, recently emerged and extensively used high-performance NFAs (such as ITIC and its derivatives) contain an electron-rich indacenodithiophene (IDT)⁴¹⁻⁴³ or indacenodithieno[3,2-*b*]thiophene (IDTT)^{27, 44-46} core and are capped with strong electron-withdrawing groups (such as phenyl-fused indanone, INCN). These NFAs typically exhibit strong absorption from 600 to 800 nm. Thus, if incorporated into PSCs, these NFAs hinder the effective harvest of photons because of the significant overlap between their absorption spectra and those of narrow-bandgap electron-donating polymers. To achieve complementary absorption in the photoactive layer, chemical modification of the core, side chains, and end-capping groups of the acceptors has been attempted to enhance the intramolecular charge transfer (ICT) effect.⁴⁷⁻⁵⁶ A series of acceptors with absorption bands broadened by introducing electron-deficient moieties have been reported and shown to enhance the harvest of solar energy when incorporated into PSCs.⁵⁰⁻⁵³ Overall, these reports suggest that enhancing the electron-withdrawing properties of the terminal groups could extend the absorption spectra of small-molecule acceptors. Thus, it is necessary to develop novel

State Key Laboratory of Luminescent Materials and Devices, Institute of Polymer Optoelectronic Materials and Devices, South China University of Technology, Guangzhou 510640, P. R. China. *E-mail: msleiyina@scut.edu.cn, E-mail: msfhuang@scut.edu.cn;

†Electronic Supplementary Information (ESI) available. See DOI: 10.1039/x0xx00000x

‡ These authors contributed equally to this work.

strong electron-withdrawing groups to produce new NFAs with extended absorption profiles. Although the effects of introducing and the complementary absorption profiles of the materials in the BHJ layer.



Scheme 1 Device architecture of non-fullerene PSCs used in the present study, and molecular structures of the donors, acceptors, and interfacial material used in the present work.

electron-accepting moieties into end-groups such as INCN have been extensively studied, less attention has been devoted to investigating the terminal groups on the optical bandgap of chromophores.

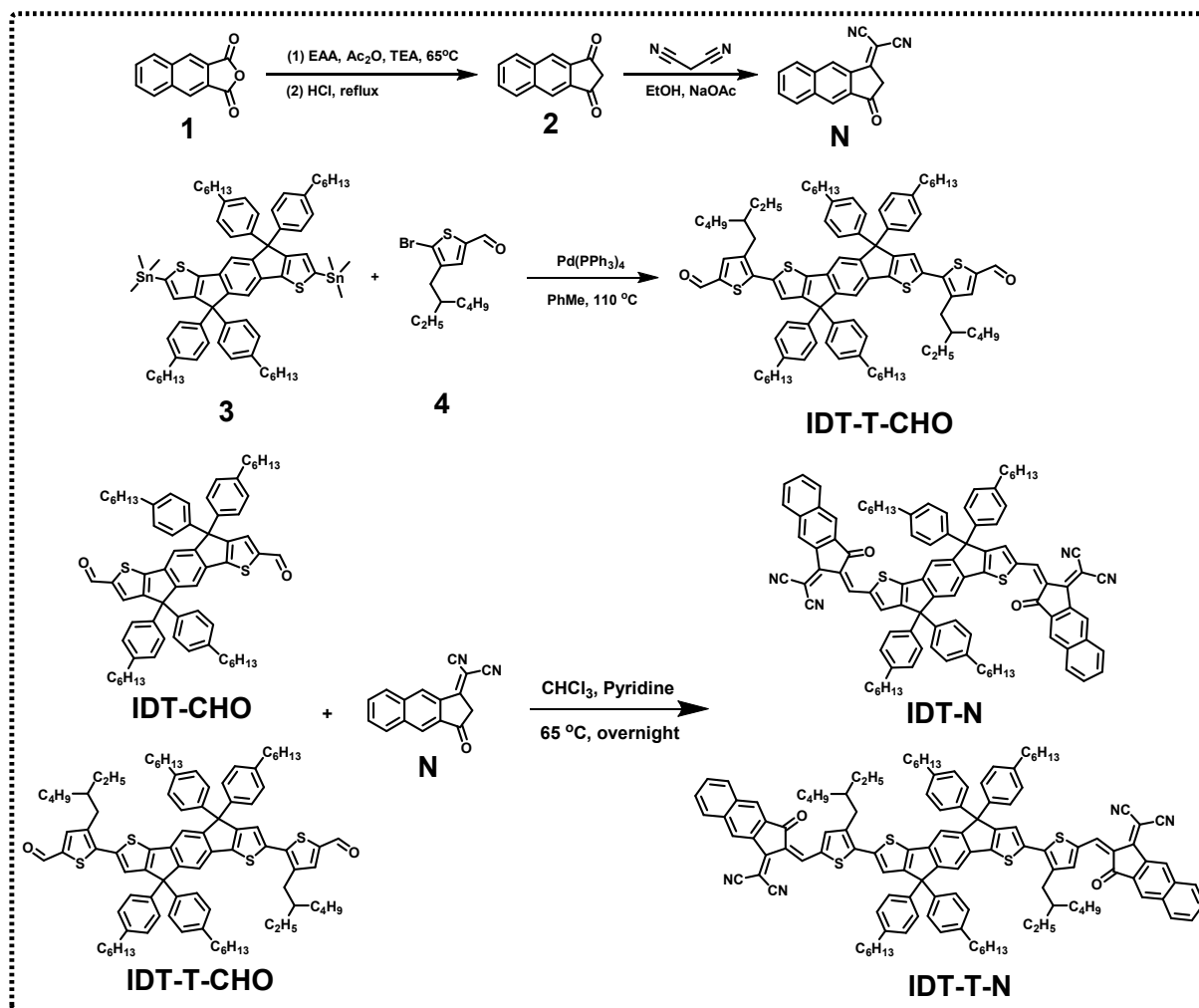
Considering that increasing the accepting strength of the end-groups can also enhance the ICT effect, resulting in red-shifted absorption spectra;⁵⁷ thus, in this study, we designed and synthesized two novel NFAs, IDT-N and IDT-T-N, which incorporate the electron-withdrawing moiety 2-(3-oxo-2,3-dihydro-1*H*-cyclopenta[*b*]naphthalen-1-ylidene)malononitrile (**N**) as the end-group and IDT as the electron-donating core unit. The electron-deficient (**N**) group exhibits expanded plane regarding to the phenyl-based indanone (INCN) and thus may enhance the intramolecular push-pull effect between the central IDT unit and the terminal acceptor unit. This may result in a reduced bandgap, thereby enhancing the light harvesting capability of PSCs and increasing the short-circuit current density (J_{sc}). IDT-T-N has a similar structure to IDT-N, with the addition of 3-(2-ethylhexyl)thiophene (T) linkers between IDT and electron-deficient (**N**) group. Both acceptors are typical low-bandgap acceptors and exhibit strong and broad absorption in the visible region and an optical bandgap of about 1.5 eV. IDT-N and IDT-T-N exhibit red-shifted absorption spectra and lower energy levels than those of IDT-IC⁴⁸ and IEIC⁴¹, respectively, which can be attributed to the enhanced electron-withdrawing properties of the naphthyl-fused indanone end-groups. PSCs fabricated using either PTB7-Th or PBDB-T as the electron-donating polymer and IDT-N or IDT-T-N as the acceptor exhibited impressive PCEs up to 9.0%. These results were attributable to the enhanced absorption of the novel NFAs

2. Results and discussion

2.1. Material synthesis and characterization

As shown in scheme 2, IDT-N and IDT-T-N were synthesized via multistep reactions using 2,3-naphthalenedicarboxylic anhydride as the starting material. First, 1*H*-cyclopenta[*b*]naphthalene-1,3(2*H*)-dione (**2**) was prepared in a 50% yield using a previously reported method.⁵⁸ The electron-withdrawing moiety 2-(3-oxo-2,3-dihydro-1*H*-cyclopenta[*b*]naphthalen-1-ylidene)malononitrile (**N**) was then synthesized (yield of 50%) by combining **2** with malononitrile in absolute ethanol at room temperature, with anhydrous sodium acetate as a catalyst. The IDT-T-CHO intermediate was obtained through a Stille coupling reaction using Pd(PPh₃)₄ as the catalyst according to a previously reported procedure.⁴¹ Finally, IDT-N and IDT-T-N were obtained via Knoevenagel condensation reactions of the intermediate compounds (IDT-CHO and IDT-T-CHO) and the electron-withdrawing (**N**) in 75% and 84% yields, respectively. The target NFAs were characterized by matrix-assisted laser desorption/ionization time of flight mass (MALDI-TOF MS) and ¹H and ¹³C nuclear magnetic resonance (NMR) spectroscopy. Both NFAs exhibited good solubility in common organic solvents, such as chloroform and *o*-dichlorobenzene. The thermal characteristics of the NFAs were evaluated by thermogravimetric analysis (TGA) in a nitrogen atmosphere (Fig. S1, ESI†). IDT-N and IDT-T-N exhibited good thermal stability, with decomposition temperatures (T_d , 5% weight loss) of 381°C and 344°C, respectively.

2.2. Theoretical calculations



Scheme 2 Synthetic routes for IDT-N and IDT-T-N.

To reveal the relationships between the geometric and electronic properties of IDT-N and IDT-T-N, their optimal ground state geometries were determined by density functional theory (DFT) calculations at the B3LYP/6-31G(d,p) level. These calculations were conducted using Gaussian 09 software. As shown in Fig. 1, the highest occupied molecular orbital (HOMO) and the lowest unoccupied molecular orbital (LUMO) are delocalized across the backbone, which correlates with the highly coplanar backbones of IDT-N and IDT-T-N. The torsion angles of the optimized geometries of IDT-N and IDT-T-N were determined to be 0.99° and 19.85°, respectively. This indicates that IDT-N has a highly planar structure that may facilitate π -electron delocalization and enhance charge mobility. It is also worth noting that the larger torsion angle of IDT-T-N may hinder π -electron delocalization and decrease charge mobility.

2.3. Optical and electrochemical properties

The normalized ultraviolet-visible (UV-Vis) absorption spectra of IDT-N and IDT-T-N in chloroform solution and as thin films are shown in Fig. 2a and 2b, respectively. The corresponding data are

summarized in Table 1. The maximum absorption peaks (λ_{\max}) of IDT-N and IDT-T-N in chloroform are located at 687 and 734 nm, respectively. The λ_{\max} peaks of IDT-N and IDT-T-N films are located at 727 and 755 nm, respectively. IDT-T-N exhibits a red-shifted λ_{\max} and a smaller optical bandgap, compared with IDT-N, because of the increased conjugation length of the core. In chloroform solution, the IDT-N spectrum exhibits shoulder absorption at 632 nm; the spectrum of IDT-T-N only has a single main absorption peak, which suggests that IDT-N has a more planar structure than IDT-T-N. This finding is consistent with the simulated molecular structure estimated by DFT.

In addition, the absorption spectra of IDT-N and IDT-T-N as thin films are slightly red-shifted compared to the corresponding solution spectra, which can be attributed to the strong π - π intermolecular interactions in thin films. The absorption peaks of IDT-N are red-shifted by 41 nm in solution and 46 nm in film relative to those of IDT-IC⁴⁸ (in which IC is electron-withdrawing capping unit); this corresponds with the slightly higher absorption coefficient of IDT-N ($1.53 \times 10^5 \text{ M}^{-1} \text{ cm}^{-1}$) relative to that of IDT-IC ($1.40 \times 10^5 \text{ M}^{-1} \text{ cm}^{-1}$). Moreover, the absorption peaks of IDT-T-N

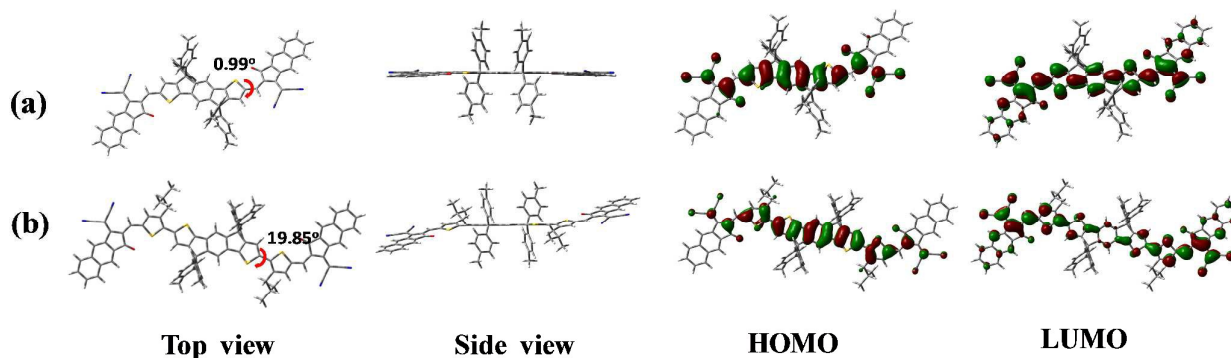


Fig. 1 Geometry of the optimized structures and frontier molecular orbitals of (a) IDT-N and (b) IDT-T-N, as determined by DFT calculations at the B3LYP/6-31G(d, p) level.

are red-shifted (by 62 nm in solution and 33 nm in film) relative to those of IEIC, and these species have similar absorption coefficients ($1.03 \times 10^5 \text{ M}^{-1} \text{ cm}^{-1}$ and $1.1 \times 10^5 \text{ M}^{-1} \text{ cm}^{-1}$). It is also worth noting that, in film state, the absorption coefficient of IDT-N ($1.49 \times 10^5 \text{ cm}^{-1}$) is much stronger than that of IDT-IC ($1.01 \times 10^5 \text{ cm}^{-1}$), while the absorption coefficient of IDT-T-N ($0.76 \times 10^5 \text{ cm}^{-1}$) is comparable to that of IEIC ($0.62 \times 10^5 \text{ cm}^{-1}$) (Fig.S4 and Table S2, ESI[†]). This trend is consistent with that observed from the chloroform solution. The difference in absorption coefficient of two systems might be originated from the molecular geometry. As the torsion angles of the central IDT unit with the end-group is relatively small for IDT-N (0.99°) and much larger for IDT-T-N (18.95°), it seems reasonable that the end-groups will have more pronounced intra-molecular charge transfer effects for IDT-N/IDT-IC. The red-shifted absorption and high absorption coefficients of IDT-N and IDT-T-N are favorable for harvesting solar photons and therefore resulting in high current densities in PSCs. The optical bandgaps of IDT-N and IDT-T-N are 1.66 and 1.52 eV, respectively, which were calculated according to the absorption edges of the thin films (784 and 854 nm, respectively).

The frontier molecular orbital energy levels of IDT-N and IDT-T-N were estimated using cyclic voltammetry (CV) with ferrocene/ferrocenium (Fc/Fc^+) as the reference (Fig. 2c). The HOMO and LUMO levels were calculated relative to the onsets of the oxidation and reduction potentials according to the following equations: $\text{HOMO} = -e [E_{\text{ox}} - E(\text{Fc}/\text{Fc}^+) + 4.8]$ (eV) and $\text{LUMO} = -e [E_{\text{red}} - E(\text{Fc}/\text{Fc}^+) + 4.8]$ (eV), where E_{ox} and E_{red} are the onsets of oxidation and reduction, respectively. The potential of the Fc/Fc^+ redox couple was surveyed at 0.2 V relative to an Ag/Ag^+ reference electrode. The CV parameters are summarized in Table 1. The HOMO/LUMO levels of IDT-N and IDT-T-N are $-5.74/-4.08$ and $-5.58/-4.06$ eV, respectively, which correspond to electrochemical bandgaps (E_{g}^{CV}) of 1.66 and 1.52 eV. IDT-T-N has an elevated LUMO level compared to IDT-N because of its greater conjugation length. This will result in a higher V_{oc} when paired with suitable donor materials. The LUMO gaps between PBDB-T and IDT-N or IDT-T-N are 0.55 and 0.53 eV, respectively, which ensure efficient exciton dissociation. However, because of the expanded plane of the electron-withdrawing moiety (N), the LUMO levels of IDT-N and IDT-T-N are lower than those of IDT-IC and IEIC, which may result in

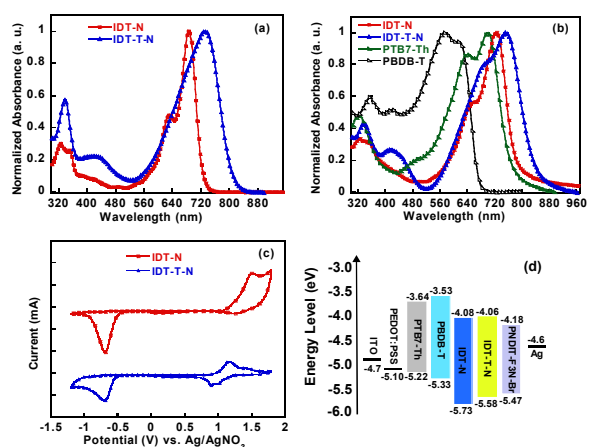


Fig. 2 Optical and electrochemical characterization of IDT-N and IDT-T-N: UV-Vis absorption spectra of the acceptors in (a) chloroform solution and (b) the acceptors and donors (PTB7-Th, PBDB-T) as films; (c) cyclic voltammetry (CV) curves; and (d) energy level diagram.

lower V_{oc} values. The energy levels of the PSCs are shown in Fig. 2d; the work functions of the ITO and Ag electrodes, and the HOMO and LUMO levels of PBDB-T, PTB7-Th, and the interlayer material (PNDIT-F3N-Br) were obtained from previous reports.^{48, 59-61}

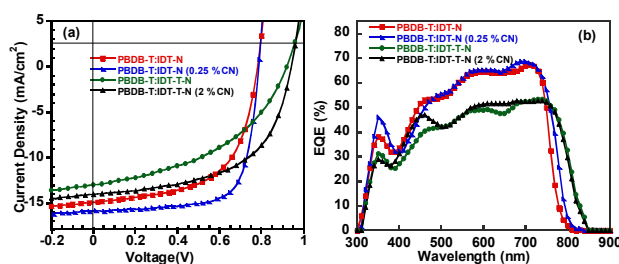
2.4. Photovoltaic properties

To investigate the photovoltaic properties of IDT-N and IDT-T-N, PSCs were fabricated in a conventional device configuration: ITO/PEDOT:PSS/active layer/PNDIT-F3N-Br/Ag, in which PNDIT-F3N-Br functioned as the cathode interlayer to facilitate the electron extraction from the active layer (Scheme 1). The active layer was composed of either a narrow bandgap polymer (PTB7-Th) or a wide bandgap polymer (PBDB-T), which acted as the electron donor material; either IDT-N or IDT-T-N was used as the electron-accepting material. The current density-voltage (J - V) curves of the studied devices are shown in Fig. 3a, and the corresponding photovoltaic parameters are summarized in Table 2. The optimization of the PSCs, including the donor:acceptor ratios and

Table 1 Optical and electrochemical properties of the two acceptors IDT-N and IDT-T-N.

	UV-vis in solution ^a		UV-vis as thin films ^b			CV ^d		
	$\lambda_{\text{max}}/\text{nm}$	$\lambda_{\text{onset}}/\text{nm}$	$\lambda_{\text{max}}/\text{nm}$	$\lambda_{\text{onset}}/\text{nm}$	$E_{\text{g}}^{\text{opt c}}/\text{eV}$	HOMO/eV	LUMO/eV	$E_{\text{g}}^{\text{cv e}}/\text{eV}$
IDT-N	687	725	727	784	1.58	-5.74	-4.08	1.66
IDT-T-N	734	812	755	854	1.45	-5.58	-4.06	1.52

^a In chloroform solution with concentration about 10^{-5} M. ^b Films were spin-coated onto a quartz plate from 10 mg mL⁻¹ chloroform solution. ^c $E_{\text{g}}^{\text{opt}} = 1240/\lambda_{\text{onset}}$. ^d Calculated HOMO/LUMO energy levels. ^e $E_{\text{g}}^{\text{cv}} = \text{LUMO} - \text{HOMO}$.

**Fig. 3** (a) J - V curves and (b) EQE spectra of devices based on PBDB-T:IDT-N, and PBDB-T:IDT-T-N devices with or without CN.

the effects of solvent additives, are summarized in Table S3 and Table S4 (ESI[†]).

The as-cast device based on PTB7-Th:IDT-N exhibited a PCE of 5.5%, which is higher than previously reported devices based on PTB7-Th:IDT-IC (3.2%). The enhanced PCE correlates to the increased J_{sc} (from 9.53 to 13.02 mA cm⁻²), which was attributed to the red-shifted and better-matched absorption of IDT-N. The devices based on PTB7-Th:IDT-T-N exhibited a PCE of 6.6%, which is higher than that of reported devices based on PTB7-Th:IEIC (6.3%)⁴¹. Devices based on PBDB-T exhibited better performances than the PTB7-Th-based PSCs, which can be attributed to the increased V_{oc} (as a result of the lower HOMO level of PBDB-T) and J_{sc} (because of better matched absorption spectra; Fig. S2, ESI[†]). The PSCs based on PBDB-T:IDT-N and PBDB-T:IDT-T-N cast without CN exhibited PCEs of 6.9% and 5.4%, respectively. Processing with 0.25% CN improved the PCE of the PBDB-T:IDT-N device from 6.9% to 9.0%; and the PCE of the PBDB-T:IDT-T-N device increased from 5.4% to 7.4% when processed with 2% CN. Hence, the addition of CN significantly enhanced photovoltaic performance by virtue of the enhanced J_{sc} and FF.

For comparison, we also fabricated devices based on IDT-IC or IEIC as the acceptor and PBDB-T as the donor, with relevant photovoltaic parameters shown in Table S5 (ESI[†], device architecture: ITO/PEDOT:PSS/active layer/PNDIT-F3N-Br/Ag). It is noted that the PCEs of devices based on PBDB-T:IDT-IC with/without CN additives are 5.7%/6.8%, and the PCEs of devices based on PBDB-T:IEIC with/without CN additives are 3.9%/6.9%, respectively. The higher PCEs of devices IDT-N and IDT-T-N are mainly due to the higher J_{sc} and FF, which can be attributed to their extended conjugation of the end-groups. We note that despite such two acceptors IDT-N and IDT-T-N exhibited similar LUMO energy level as estimated by CV measurement, the resulting device based on IDT-T-N exhibited obviously higher V_{oc} than those of device

Table 2 Photovoltaic parameters of the PSCs based on PTB7-Th or PBDB-T as donors and IDT-N or IDT-T-N as acceptors under AM 1.5 G illumination at 100 mW cm⁻².

Active layer	CN (vol%) additive	V_{oc} (V)	J_{sc} (mA cm ⁻²)	FF (%)	PCE (%)
PTB7-Th:IDT-IC	w/o	0.83	9.53	40.0	3.2 ^a
PTB7-Th:IEIC	w/o	0.97	13.55	48.0	6.3 ^a
PTB7-Th:IDT-N	w/o	0.73	13.02	57.70	5.5
PTB7-Th:IDT-T-N	2 %	0.87	14.67	51.38	6.6
PBDB-T:IDT-N	w/o	0.78	14.89	59.12	6.9
PBDB-T:IDT-N	0.25 %	0.79	15.88	71.91	9.0
PBDB-T:IDT-T-N	w/o	0.92	12.97	44.79	5.4
PBDB-T:IDT-T-N	2 %	0.94	14.03	56.11	7.4

^a Data from previous reports.^{41,48}

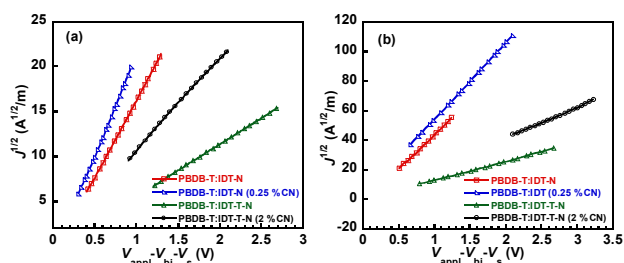
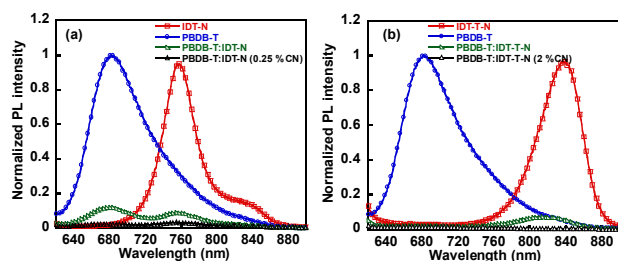
based on IDT-N. However, as V_{oc} correlates with a range of factors such as charge transfer state, film morphology, tail of density of state, and so forth, at the current stage it is not clear which is the dominant factor that determines the loss of V_{oc} . Nevertheless, it is worth pointing out that the device based on PBDB-T:IDT-T-N exhibits a relatively small energy losses ($E_{\text{loss}} = E_{\text{g}} - eV_{\text{oc}}$) of 0.51 eV, which is slightly larger than those for inorganic solar cells (0.35-0.50 eV)⁶² whilst smaller than the typical values of 0.6-1.0 eV for PSCs.

The external quantum efficiency (EQE) curves of the devices based on PBDB-T:IDT-N or PBDB-T:IDT-T-N with or without CN are shown in Fig. 3b. The EQE responses are consistent with the measured J_{sc} values of the devices. The integrated photocurrents were 14.52 and 15.17 mA cm⁻² for the PBDB-T:IDT-N system without and with CN additive, respectively, which are very close to those of 14.89 and 15.88 mA cm⁻² obtained from the J - V characterization, respectively (Table 2). Similarly, the integrated photocurrents were 12.81 and 13.15 mA cm⁻² for the PBDB-T:IDT-T-N system without and with CN additive, respectively, which are also close to those of 12.97 and 14.03 mA cm⁻² obtained from the J - V characterization respectively (Table 2). The PBDB-T:IDT-N systems exhibited a broad photoresponse from 300 to 780 nm with a maximum value of about 69% at 700 nm. The PBDB-T:IDT-T-N systems had a broader response, from 300 to 850 nm, with a maximum value of about 53% at 730 nm. These results are in good agreement with the UV-Vis absorption spectra of the acceptors and the PBDB-T donor (Fig. S2, ESI[†]).

ARTICLE

Table 3 Electron/hole mobility for PBDB-T:acceptor blend films and pristine acceptor films.

Film	μ_e ($\text{cm}^2 \text{V}^{-1} \text{s}^{-1}$)	μ_h ($\text{cm}^2 \text{V}^{-1} \text{s}^{-1}$)	μ_h/μ_e
PBDB-T:IDT-N	1.72×10^{-4}	3.76×10^{-4}	2.19
PBDB-T:IDT-N (0.25 % CN)	2.87×10^{-4}	4.57×10^{-4}	1.59
PBDB-T:IDT-T-N	1.96×10^{-5}	5.58×10^{-5}	2.85
PBDB-T:IDT-T-N (2 % CN)	6.07×10^{-5}	1.43×10^{-4}	2.36
IDT-N	1.09×10^{-4}		
IDT-T-N	1.53×10^{-5}		

**Fig. 4** (a) Electron-only and (b) hole-only $J^{1/2}$ - V characteristics of PBDB-T:IDT-N and PBDB-T:IDT-T-N blend films with or without CN.**Fig. 5** PL spectra of thin films: (a) PBDB-T, IDT-N and PBDB-T:IDT-N (1:1, w/w, without and with 0.25% CN); (b) PBDB-T, IDT-T-N and PBDB-T:IDT-T-N (1:1, w/w, without and with 2% CN).

Space-charge limited current (SCLC) methods were used to evaluate the charge carrier mobilities of the pristine IDT-N and IDT-T-N films and the PBDB-T:IDT-N and PBDB-T:IDT-T-N blend films with and without CN. The electron-only and hole-only mobilities were measured using devices with ITO/Al/BHJ film/Ca/Al and ITO/PEDOT:PSS/BHJ film/MoO₃/Ag architectures, respectively. The current-voltage ($J^{1/2}$ - V) curves of these devices are shown in Fig. 4 and Fig. S5 (ESI[†]). The electron mobilities of the IDT-N and IDT-T-N films were calculated as 1.09×10^{-4} and $1.53 \times 10^{-5} \text{ cm}^2 \text{V}^{-1} \text{s}^{-1}$ (Table 3), respectively. The addition of CN increased the electron and hole mobilities of both blend films, which correlates with the increased J_{SC} values of these devices. Furthermore, the μ_h/μ_e ratios of the blend films processed with CN (1.59 and 2.36 for PBDB-T:IDT-N and PBDB-T:IDT-T-N, respectively) were found to be lower than those of the devices processed without CN (2.19 and 2.85, respectively). The more balanced hole/electron ratios suppressed bimolecular recombination and increased the FF values of the CN-

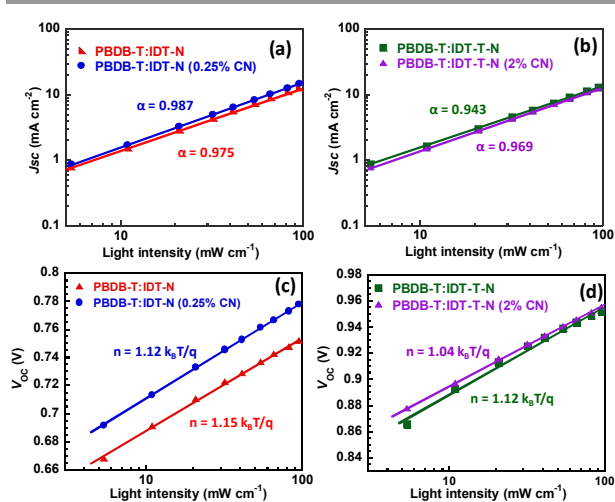
processed films, which is consistent with the results of previous experiments. These findings indicated that the addition of CN is an efficient way to improve the morphologies, charge mobilities, and FF values of blend films.

2.5. Charge transfer and recombination

Photoluminescence (PL) measurements of the BHJ films were performed to monitor charge transfer between the donor and acceptor materials. The fluorescence spectra of pure IDT-N, IDT-T-N, and PBDB-T and pristine and optimized PBDB-T:IDT-N and PBDB-T:IDT-T-N blend films are shown in Fig. 5a and 5b, respectively. The blend films processed with chloronaphthalene (CN) as a solvent additive exhibited more effective PL quenching than the pristine films. This suggests that more effective photoinduced charge transfer occurred between PBDB-T and the acceptors (IDT-N and IDT-T-N), in the blend films processed with CN, and nearly all of the excitons were dissociated. This is beneficial for achieving a higher J_{SC} in PSCs fabricated from these films.

To understand the charge recombination mechanism of the studied devices, we investigated the characteristics of J_{SC} and V_{OC} as a function of light intensity (P_{light}) that varied from 5 to 100 mW cm^{-2} . The relevant characteristics are plotted in Fig. 6. The power law dependence of J_{SC} upon illumination intensity can be expressed as $J_{SC} \propto (P_{light})^S$. Here S is the exponential factor. It is noted that the J_{SC} of the fabricated devices increased linearly with P_{light} (Fig. 6a and b). The extracted S value slightly increased from 0.975 (without CN) to 0.987 (with CN) for the device based on IDT-N (Fig. 6a), and the S value also slightly increased from 0.943 (without CN) to 0.969 (with CN) for the device based on IDT-T-N (Fig. 6b). These results demonstrate that the bimolecular recombination can be suppressed in devices processed with CN, which can lead to improved FF.

Moreover, we plotted the V_{OC} as a function of P_{light} . The slope of V_{OC} versus the natural logarithm of P_{light} gives a value of $k_B T/q$, where k_B , T , and q represent the Boltzmann constant, temperature

**Fig. 6** (a), (b) J_{SC} as a function of light intensity and (c), (d) V_{OC} as a function of light intensity for the devices based on PBDB-T:IDT-N or PBDB-T:IDT-T-N with or without CN additives, respectively.

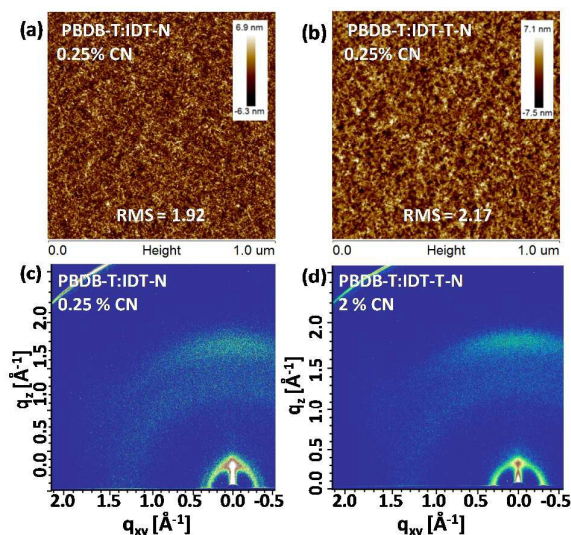


Fig. 7 AFM height images ($1 \times 1 \mu\text{m}$) and 2D-GIXD patterns of PBDB-T:IDT-N (a and c, 0.25% CN) and PBDB-T:IDT-T-N (b and d, 2% CN) blend films.

(K), and elementary charge, respectively. It is noted that the extracted slope of IDT-N based device slightly decreased from $1.15 k_B T/q$ (without CN) to $1.12 k_B T/q$ (with CN) (Fig. 6c), and the extracted slope of IDT-T-N based device also slightly decreased from $1.12 k_B T/q$ (without CN) to $1.04 k_B T/q$ (with CN) (Fig. 6d). Typically, when the additional mechanism such as trap-assisted recombination is involved, a stronger dependence of V_{OC} on P_{light} with a slope greater than $k_B T/q$ can be observed. The obtained lower slope demonstrates the reduced trap density and suppressed trap-assisted recombination in the devices processed with CN additive.

2.6. Film morphology

The film morphology was investigated by using atomic force microscopy (AFM), transmission electron microscopy (TEM), and grazing incidence wide angle X-ray diffraction (GIWAXS). Regarding to the PBDB-T:IDT-N and PBDB-T:IDT-T-N films (Fig. S6, ESI), the blend films processed with solvent additive of CN exhibited fibrous features with slightly larger root-mean-square (RMS) values (Fig. 7a, b). Additionally, from the TEM images one can note more obvious phase separation of the CN-processed film than those processed without additive (Fig. S7, ESI). GIWAXS was used to investigate the molecular ordering in the neat films as well as the blends. One can obviously note that both the neat films of IDT-N and IDT-T-N exhibited strong (010) diffraction peaks in the out-of-plane (OOP) direction and the corresponding (100) peaks in the in-plane (IP) direction (Fig S8a, b and g), which indicates the formation of the predominant "face-on" orientation of these acceptors. For blends, the (010) reflection peaks located at 1.80 \AA^{-1} in OOP direction and the corresponding (100) peaks at 0.31 \AA^{-1} in IP direction, demonstrating that the preferential "face-on" orientation, which is favorable for vertical charge transportation. It is also worth noting that the intensity of the (100) peaks at 0.31 \AA^{-1} in OOP direction are stronger for blends processed with CN additives, which indicates

the improved alky side chain stacking. This observation was consistent with the enhanced photovoltaic performance of devices processed with CN additives compared with those processed without CN.

3. Conclusion

Two novel NFAs (IDT-N and IDT-T-N) based on an IDT core end-capped with the electron-withdrawing moiety 2-(3-oxo-2,3-dihydro-1*H*-cyclopenta[*b*]naphthalen-1-ylidene)malononitrile (N) were designed and synthesized. The terminal (N) groups enhanced the electron acceptance of the NFAs, relative to those terminated with phenyl-fused indanone moieties. Moreover, IDT-N and IDT-T-N exhibit red-shifted absorption, deeper LUMO levels, and smaller bandgaps than IDT-IC and IEIC, respectively. The broadened and red-shifted optical absorption of the novel NFAs resulted in improved J_{SC} values for the corresponding PSCs. However, because of their decreased LUMO energy levels, the V_{OC} values of the PSCs were relatively low. The devices based on PBDB-T:IDT-N exhibited the highest measured PCE (9.0%). The devices based on PBDB-T:IDT-T-N exhibited a moderate PCE of 7.4%. When the narrow bandgap copolymer PTB7-Th was used as the electron-donating material, the resulting IDT-N- and IDT-T-N-based PSCs exhibited higher performances than those based on either IDT-IC or IEIC. Overall, the results of this study demonstrate that novel small molecule acceptors are promising candidates as replacements for fullerene derivatives in PSCs and that the modification of end-group units is a promising strategy to develop more efficient non-fullerene acceptors.

4. Experimental section

4.1. General information

All reactions were carried out under argon atmosphere. All solvents and reagents were commercially available and used directly without further purification unless otherwise specified. Tetrahydrofuran (THF) and toluene (PhMe) were dried from sodium/benzophenone and freshly distilled before to use. NMR spectra were recorded with a 500 MHz NMR spectrometer for ^1H NMR and 125 MHz for ^{13}C NMR with tetramethylsilane (TMS) as the internal reference. MALDI-TOF-MS spectra was measured on a BrukerBIFLEXIII mass spectrometer. UV-vis spectra was performed by using a HP 8453 spectrophotometer. Thermogravimetric analyses (TGA) were recorded on a NETZSCH TG 209 at a heating rate of $10 \text{ }^\circ\text{C min}^{-1}$ under a nitrogen flow rate of 20 mL min^{-1} . The electrochemical cyclic voltammetry (CV) experiments were carried out on a CHI600D electrochemical workstation equipped with a ITO working electrode, a platinum wire counter electrode, a Ag/AgNO₃ reference electrodes and a 0.1 mol L⁻¹ acetonitrile solution of tetrabutylammoniumhexafluorophosphate (n-Bu₄NPF₆) as the supporting electrolyte at a scan rate of 100 mV s^{-1} under a nitrogen atmosphere. The ferrocene/ferrocenium redox couple (Fc/Fc⁺) was used to calibrate the potential of Ag/AgNO₃ reference electrode. The atomic force microscopy

(AFM) measurements were carried out on a NanoMan VS microscope with a tapping mode. TEM images were obtained from a JEM-2100F instrument. The geometry of the acceptors were optimized by using Density Functional Theory (DFT) method at a B3LYP/6-31G(d) level to optimize the ground state geometries. All the calculations of the acceptor molecules were performed using the Gaussian 09 package package40, all the straight-chain substituents were replaced with methyl groups and the branched side-chain substituents were replaced with isopropyl groups for calculations.

4.2. Synthesis

Synthesis of compound (2). In a dried two-neck 100 mL flask. Naphtho[2,3-c]furan-1,3-dione (**1**) (10 g, 50.5 mmol) was dissolved in acetic anhydride (30 mL), and triethylamine (20 mL) was added under an argon atmosphere. After stirred for a while, ethylacetoacetate (19.6 mL, 151.5 mmol) was quickly added via a syringe and the reaction was stirred at 100 °C for 12 h. The reaction mixture was cooled to room temperature and poured into HCl (2N) with ice, the resulting yellow precipitate was collected by filtration and washed with water, and then the yellow residual dissolved in HCl (5N) was heated under reflux for 1h. After being cooled to room temperature, the solid crude product was collected by filtration, washed with water and then purified by flash chromatography (CH₂Cl₂). Yield: 50 %. ¹H NMR (500 MHz, CDCl₃, δ): 8.50 (s, 2H), 8.12-8.10 (m, 2H), 7.74-7.72 (m, 2H), 3.37(s, 2H); ¹³C NMR (125 MHz, CDCl₃, δ): 197.70, 138.17, 136.36, 130.66, 129.72, 124.31, 46.69.

Synthesis of compound (N). In a dried two-neck 100 mL flask. 1*H*-Cyclopenta[*b*]naphthalene-1,3(2*H*)-dione (**2**) (2.5g, 12.76 mmol), malononitrile (5.05 g, 76.53 mmol) were dissolved in ethanol (50 mL), and then anhydrous sodium acetate (4.18 g, 0.51 mmol) was slowly added while stirring. After stirred 2h, the reaction mixture was poured into ice-water, and acidified to PH 1-2 by addition of hydrochloric acid. The resulting precipitate was collected by filtration and washed with water, the crude product was purified by flash chromatography (CH₂Cl₂) and recrystallized from n-hexane to gave the target product 2-(3-oxo-2,3-dihydro-1*H*-cyclopenta[*b*]naphthalen-1-ylidene)malononitrile (**N**). Yield: 50 %. ¹H NMR (500 MHz, CDCl₃, δ): 9.18 (s, 1H), 8.49 (s, 1H), 8.17-8.10 (m, 2H), 7.81-7.78 (m, 2H), 3.85(s, 2H); ¹³C NMR (125 MHz, CDCl₃, δ): 187.16, 162.36, 137.27, 136.22, 134.66, 134.05, 129.88, 129.57, 127.78, 127.58, 121.05, 119.94, 119.06, 106.48, 67.49, 25.59. MS (ESI): calcd for C₁₆H₈N₂O [M⁺], 244.1; found: 245.6. Anal. calcd for C₁₆H₈N₂O: C 78.68, H 3.30, N 11.47; found: C 78.54, H 3.19, N 11.42.

Synthesis of IDT-T-CHO. To a two-necked round bottom flask compound **4** (500 mg, 0.41 mmol), compound **5** (345 mg, 1.22 mmol), Pd(PPh₃)₄ (70 mg, 0.06 mmol) and toluene (50 mL) were added. The mixture was deoxygenated with nitrogen for 30 min. The mixture was refluxed for 72 h and then was allowed to cool down to room temperature. After removing the solvent from the filtrate, the residue was purified using column chromatography on a silica gel employing

dichloromethane/petroleum ether (1:1) as an eluent, yielding an orange solid (395 mg, 70%). ¹H NMR (500 MHz, CDCl₃, δ): 9.80 (s, 2H), 7.52 (s, 2H), 7.45 (s, 2H), 7.18 (s, 2H), 7.16 (d, *J* = 8.4 Hz, 8H), 7.07 (d, *J* = 8.4 Hz, 8H), 2.72 (d, *J* = 8.4 Hz, 4H), 2.56 (t, *J* = 8.4 Hz, 8H), 1.67 (m, 2H), 1.60 (m, 8H), 1.29 (m, 40H), 0.87 (m, 24H).

Synthesis of IDT-N. IDT-CHO (100mg, 0.104mmol), N (126mg, 0.519mmol), chloroform (30 mL), and pyridine (0.5 mL) were added to a two-necked round-bottomed flask, the mixture was deoxygenated with argon for 20 min and then stirred overnight at 65 °C. After cooling to room temperature, the solvent was removed under vacuum. The crude product was purified by column chromatography on a silica gel using dichloromethane as an eluent and then recrystallization from chloroform/methanol to afford TDT-N as a deep blue solid (110mg, 75%). ¹H NMR (500 MHz, CDCl₃, δ): 9.19 (s, 2H), 8.97 (s, 2H), 8.36 (s, 2H), 8.07-8.04 (m, 4H), 7.76 (s, 2H), 7.69-7.66 (m, 4H), 7.18-7.13 (m, 16H), 2.61-2.58 (t, *J* = 7.5 Hz, 8H), 1.64-1.58 (m, 8H), 1.37-1.26 (m, 24H), 0.88-0.86 (t, *J* = 5Hz, 12H); ¹³C NMR (125 MHz, CDCl₃, δ): 188.28, 160.25, 159.45, 158.23, 156.55, 142.42, 142.08, 140.30, 139.75, 138.82, 137.29, 136.29, 135.42, 134.64, 132.83, 130.68, 130.22, 129.96, 129.69, 128.82, 127.66, 127.03, 124.65, 124.41, 120.15, 115.19, 115.01, 68.09, 63.01, 35.58, 31.72, 31.33, 29.09, 22.60, 14.12. MS (MALDI-TOF) calcd for C₉₈H₈₆N₄O₂S₂, 1414.6192; found, 1415.241. Anal. calcd for C₉₈H₈₆N₄O₂S₂: C 83.13, H 6.12, N 3.96, S 4.53; found: C 83.29, H 6.27, N 3.91, S 4.65.

Synthesis of IDT-T-N. The synthetic routes of IDT-T-N are similar to that of IDT-N. IDT-T-CHO (200mg, 0.148mmol), N (181mg, 0.741mmol), chloroform (30 mL), and pyridine (1.0 mL) were added to a two-necked round-bottomed flask, the mixture was deoxygenated with argon for 20 min and then stirred overnight at 65 °C. After cooling to room temperature, the solvent was removed under vacuum. The crude product was purified by column chromatography on a silica gel using dichloromethane as an eluent and then recrystallization from chloroform/methanol to afford IDT-T-N as a deep green solid (224 mg, 84% yield) ¹H NMR (500 MHz, CDCl₃, δ): 9.16 (s, 2H), 8.84 (s, 2H), 8.36 (s, 2H), 8.07-8.00 (m, 4H), 7.69-7.65 (m, 4H), 7.61 (s, 2H), 7.52 (s, 2H), 7.50 (s, 2H), 7.22 (d, *J* = 10Hz, 8H), 7.13 (d, *J* = 10Hz, 8H), 2.79 (d, *J* = 10Hz, 4H), 2.60 (t, *J* = 7.5Hz, 8H), 1.79-1.72 (m, 2H), 1.65-1.59 (m, 8H), 1.40-1.26 (m, 40H), 0.89-0.85 (t, *J* = 5Hz, 24H); ¹³C NMR (125 MHz, CDCl₃, δ): 188.39, 160.29, 157.54, 154.37, 151.01, 149.42, 145.46, 141.98, 141.06, 140.12, 138.08, 137.68, 136.22, 135.37, 134.77, 134.59, 132.85, 130.62, 130.20, 129.82, 129.58, 128.61, 127.89, 126.84, 124.60, 124.48, 124.00, 118.05, 115.32, 115.13, 67.78, 63.17, 39.32, 35.61, 33.83, 32.44, 31.74, 31.38, 29.14, 28.59, 25.67, 23.05, 22.60, 14.13, 14.11, 10.58. MS (MALDI-TOF) calcd for C₁₂₂H₁₂₂N₄O₂S₄, 1802.8451; found, 1803.423. Anal. calcd for C₁₂₂H₁₂₂N₄O₂S₄: C 81.00, H 6.81, N 3.10, S 7.11; found: C 80.85, H 6.93, N 2.95, S 7.29.

4.3. Fabrication and characterization of solar cells

All the solar cell devices with a conventional configuration of ITO/PEDOT:PSS/active layer/PNDIT-F3N-Br/Ag were fabricated.

Firstly, the ITO glass substrates were pre-cleaned sequentially by using detergent, ethanol, acetone, and isopropyl alcohol under sonication, and dried in oven at 70 °C for 10 h before to use. Followed by treating with oxygen plasma for 4 min, the PEDOT:PSS was spin-coated onto the ITO glass at 3000 rpm for 30 s and then annealed at 150 °C for 10 min in air. Subsequently, the substrates were transferred into a N₂-protected glove box for spin-coating the active layer. The donor polymer (PTB7-Th or PBDB-T) and the small molecule acceptor (IDT-N or IDT-T-N) were dissolved in CHCl₃ solution (with variant blend ratios, the total concentration of the donor polymer and the acceptor is 10 mg mL⁻¹). The mixed solution was spin-coated atop the PEDOT:PSS layer at 2000 rpm for 30 s to form the active layer with a film thicknesses approximately 100 nm. Then, the active layers were treated with thermal annealing at 100 °C for 10 min. Finally, the interface layer (5 nm) of PNDIT-F3N-Br in methanol (0.5mg mL⁻¹) was spin-coated on the blended films, and then the top electrode silver (100 nm) was deposited onto the interlayer PNDIT-F3N-Br by thermal evaporation through a shadow mask in a vacuum chamber with a base pressure of 1×10⁻⁶ mbar. The active layer area of the device was 0.04 cm². The current density-voltage (*J*-*V*) characteristics were recorded using a computer-controlled Keithley 2400 source meter under an AM 1.5G solar simulator (Taiwan, Enlitech SS-F5) at a light intensity of 100 mW cm⁻², which was tested by a calibrated silicon solar cell (certified by National Renewable Energy Laboratory) before to test. The PL spectra and EQE spectra were performed on a FLS920 spectro-fluorimeter (Edinburgh Instruments) and a commercial EQE measurement system (Taiwan, Enlitech, QE-R), respectively.

4.4. SCLC measurements

The hole-only and electron-only mobilities of PBDB-T: acceptors blend films and the acceptor neat films were determined from space-charge-limited current (SCLC) devices. The devices were fabricated with the structures of ITO/Al/blend films (or neat film)/Ca/Al for electron-only mobility and ITO/PEDOT:PSS/blend films (neat film)/MoO₃/Ag for hole-only mobility, respectively. The mobilities were determined by fitting the dark *J*-*V* current to the model of a single carrier SCLC which were calculated on the basis of the following equation:

$$J = \frac{9}{8} \epsilon_0 \epsilon_r \mu_h \frac{V^2}{d^3}$$

where *J* is the current, ε₀ and ε_r are the permittivity of free space and relative permittivity of the material, respectively, and μ_h, *V* and *d* are the zero-filled mobility, the effective voltage, and the thickness of the organic layer, respectively. The effective voltage can be obtained from the equation *V* = *V*_{appl} - *V*_{bi} - *V*_s, where *V*_{appl}, *V*_{bi} and *V*_s are the applied voltage, the offset voltage and the voltage drop, respectively, (*V*_{bi} = 0 and *V*_s = 10×*I*, where the value 10 is the resistance of MnO₃ and *I* is the current of the devices in this work). The electron- and hole-mobility can be calculated from the slope of the *J*^{1/2}-*V* curves.

Acknowledgements

This work was financially supported by the Ministry of Science and Technology of China (No. 2014CB643501), the Natural Science Foundation of China (No. 91633301, 51673069, 21634004, 21520102006 and 21761132001), Foundation of Guangzhou Science and Technology Project (201607020010 and 201707020019), and Fundamental Research Funds for the Central Universities (SCUT).

Notes and references

- 1 G. Yu, J. Gao, J. C. Hummelen, F. Wudl and A. J. Heeger, *Science*, 1995, **270**, 1789.
- 2 Y.-J. Cheng, S.-H. Yang and C.-S. Hsu, *Chem. Rev.*, 2009, **109**, 5868.
- 3 Z. Hu, L. Ying, F. Huang and Y. Cao, *Sci. China Chem.*, 2017, **60**, 571.
- 4 B. Xiao, A. Tang, J. Zhang, A. Mahmood, Z. Wei and E. Zhou, *Adv. Energy Mater.*, 2017, **7**, 1602269.
- 5 Z. Liu, Y. Wu, Q. Zhang and X. Gao, *J. Mater. Chem. A*, 2016, **4**, 17604.
- 6 S. Guenes, H. Neugebauer and N. S. Sariciftci, *Chem. Rev.*, 2007, **107**, 1324.
- 7 L. Ye, S. Zhang, L. Huo, M. Zhang and J. Hou, *Acc. Chem. Res.*, 2014, **47**, 1595.
- 8 J. Yuan, M. J. Ford, Y. Zhang, H. Dong, Z. Li, Y. Li, T. Q. Nguyen, G. C. Bazan and W. Ma, *Chem. Mater.*, 2017, **29**, 1758.
- 9 D. Dang, W. Chen, S. Himmelberger, Q. Tao, A. Lundin, R. Yang, W. Zhu, A. Salleo, C. Müller and E. Wang, *Adv. Energy Mater.*, 2014, **4**, 1400680.
- 10 L. Lan, Z. Chen, Q. Hu, L. Ying, R. Zhu, F. Liu, T. P. Russell, F. Huang and Y. Cao, *Adv. Sci.*, 2016, **3**, 1600032.
- 11 C. Chen, W. Chang, K. Yoshimura, K. Ohya, J. You, J. Gao, Z. Hong and Y. Yang, *Adv. Mater.*, 2014, **26**, 5670.
- 12 H. Zhou, Y. Zhang, C. K. Mai, S. D. Collins, G. C. Bazan, T. Q. Nguyen and A. J. Heeger, *Adv. Mater.*, 2015, **27**, 1767.
- 13 L. Nian, K. Gao, F. Liu, Y. Kan, X. Jiang, L. Liu, Z. Xie, X. Peng, T. P. Russell and Y. Ma, *Adv. Mater.*, 2016, **28**, 8184.
- 14 K. H. Park, Y. Ana, S. Jung, H. Park and C. Yang, *Energy Environ. Sci.*, 2016, **9**, 3464.
- 15 J. Zhao, Y. Li, G. Yang, K. Jiang, H. Lin, H. Ade, W. Ma and H. Yan, *Nat. Energy*, 2016, **1**, 15027.
- 16 G. Zhang, K. Zhang, Q. Yin, X.-F. Jiang, Z. Wang, J. Xin, W. Ma, H. Yan, F. Huang and Y. Cao, *J. Am. Chem. Soc.*, 2017, **139**, 2387.
- 17 B. Fan, K. Zhang, X. Jiang, L. Ying, F. Huang and Y. Cao, *Adv. Mater.*, 2017, **29**, 1606396.
- 18 G. Ding, J. Yuan, F. Jin, Y. Zhang, L. Han, X. Ling, H. Zhao and W. Ma, *Nano Energy*, 2017, **36**, 356.
- 19 B. Azzopardi, C. J. M. Emmott, A. Urbina, F. C. Krebs, J. Mutale and J. Nelson, *Energy Environ. Sci.*, 2011, **4**, 3741.
- 20 A. Tournebize, P. O. Bussière, A. Rivaton, J. L. Gardette, H. Medlej, R. C. Hiorns, C. Dagnonlartigau, F. C. Krebs and K. Norrman, *Chem. Mater.*, 2013, **25**, 4522.
- 21 B. Fan, L. Ying, Z. Wang, B. He, X. Jiang, F. Huang and Y. Cao, *Energy Environ. Sci.*, 2017, **10**, 1243.
- 22 C. Dou, Z. Ding, Z. Zhang, Z. Xie, J. Liu and L. Wang, *Angew. Chem. Int. Ed.*, 2015, **54**, 3648.
- 23 C. Zhang, A. Mumyatov, S. Langner, J. D. Perea, T. Kassar, J. Min, L. Ke, H. Chen, K. L. Gerasimov, D. V. Anokhin, D. A. Ivanoy, T.

ARTICLE

Journal Name

- Ameri, A. Osvet, D. K. Susarova, T. Unruh, N. Li, P. Troshin and C. J. Brabec, *Adv. Energy Mater.*, 2017, **7**, 1601204.
- 24 D. Meng, D. Sun, C. Zhong, T. Liu, B. Fan, L. Huo, Y. Li, W. Jiang, H. Choi, T. Kim, J. Y. Kim, Y. Sun, Z. Wang and A. J. Heeger, *J. Am. Chem. Soc.*, 2016, **138**, 375.
- 25 Y. Li, L. Zhong, B. Gautam, H. Bin, J. Lin, F. Wu, Z. Zhang, Z. Jiang, Z. Zhang, K. Gundogdu, Y. Li and L. Liao, *Energy Environ. Sci.*, 2017, **10**, 1610.
- 26 W. Su, Q. Fan, X. Guo, B. Guo, W. Li, Y. Zhang, M. Zhang and Y. Li, *J. Mater. Chem. A*, 2016, **4**, 14752.
- 27 Y. Lin, J. Wang, Z. G. Zhang, H. Bai, Y. Li, D. Zhu and X. Zhan, *Adv. Mater.*, 2015, **27**, 1170.
- 28 S. Li, J. Yan, C. Li, F. Liu, M. Shi, H. Chen and T. P. Russell, *J. Mater. Chem. A*, 2016, **4**, 3777.
- 29 F. Liu, Z. Zhou, C. Zhang, T. Vergote, H. Fan, F. Liu and X. Zhu, *J. Am. Chem. Soc.*, 2016, **138**, 15523.
- 30 N. Qiu, H. Zhang, X. Wan, C. Li, X. Ke, H. Feng, B. Kan, H. Zhang, Q. Zhang, Y. Lu and Y. Chen, *Adv. Mater.*, 2017, **29**, 1604964.
- 31 S. Chen, G. Zhang, J. Liu, H. Yao, J. Zhang, T. Ma, Z. Li and H. Yan, *Adv. Mater.*, 2017, **29**, 1604231.
- 32 Y. Cui, H. Yao, B. Gao, Y. Qin, S. Zhang, B. Yang, C. He, B. Xu and J. Hou, *J. Am. Chem. Soc.*, 2017, **139**, 7302.
- 33 C. Pei, M. Zhang, T. K. Lau, W. Yao, B. Jia, J. Wang, C. Yan, Q. Meng, X. Lu and X. Zhan, *Adv. Mater.*, 2017, **29**, 1605216.
- 34 A. Zhang, C. Li, F. Yang, J. Zhang, Z. Wang, Z. Wei and W. Li, *Angew. Chem. Int. Ed.*, 2017, **56**, 2694.
- 35 Z. Zhang, M. Li, Y. Liu, J. Zhang, S. Feng, X. Xu, J. Song and Z. Bo, *J. Mater. Chem. A*, 2017, **5**, 7776.
- 36 W. Wang, C. Yan, T. K. Lau, J. Wang, K. Liu, Y. Fan, X. Lu and X. Zhan, *Adv. Mater.*, 2017, **29**, 1701308.
- 37 S. Li, L. Ye, W. Zhao, S. Zhang, H. Ade and J. Hou, *Adv. Energy Mater.*, 2017, **7**, 1700183.
- 38 S. Zhang and J. Hou, *Acta Phys. -Chim. Sin.*, 2017, **33**, 2327.
- 39 W. Zhao, L. Ye, S. Li, X. Liu, S. Zhang, Y. Zhang, M. Ghasemi, C. He, H. Ade and J. Hou, *Sci. China Mater.*, 2017, **60**, 697.
- 40 W. Zhao, S. Li, H. Yao, S. Zhang, Y. Zhang, B. Yang and J. Hou, *J. Am. Chem. Soc.*, 2017, **139**, 7148.
- 41 Y. Lin, Z. Zhang, H. Bai, J. Wang, Y. Yao, Y. Li, D. Zhu and X. Zhan, *Energy Environ. Sci.*, 2015, **8**, 610.
- 42 Y. Wu, H. Bai, Z. Wang, P. Cheng, S. Zhu, Y. Wang, W. Ma and X. Zhan, *Energy Environ. Sci.*, 2015, **8**, 3215.
- 43 H. Lin, S. Chen, Z. Li, J. Y. Lai, G. Yang, T. McAfee, K. Jiang, Y. Li, Y. Liu, H. Hu, J. Zhao, W. Ma, H. Ade and H. Yan, *Adv. Mater.*, 2016, **27**, 7299.
- 44 H. Bin, Z. G. Zhang, L. Gao, S. Chen, L. Zhong, L. Xue, C. Yang and Y. Li, *J. Am. Chem. Soc.*, 2016, **138**, 4657.
- 45 Y. Lin, F. Zhao, Q. He, L. Huo, Y. Wu, T. C. Parker, W. Ma, Y. Sun, C. Wang, D. Zhu, A. J. Heeger, S. R. Marder and X. Zhan, *J. Am. Chem. Soc.*, 2016, **138**, 4955.
- 46 W. Zhao, D. Qian, S. Zhang, S. Li, O. Inganäs, F. Gao and J. Hou, *Adv. Mater.*, 2016, **28**, 4734.
- 47 Y. Lin, T. Li, F. Zhao, L. Han, Z. Wang, Y. Wu, Q. He, J. Wang, L. Huo, Y. Sun, C. Wang, W. Ma and X. Zhan, *Adv. Energy Mater.*, 2016, **6**, 1600854.
- 48 Y. Li, X. Liu, F. P. Wu, Y. Zhou, Z. Q. Jiang, B. Song, Y. Xia, Z. G. Zhang, F. Gao, O. Inganäs, Y. Li and L. Liao, *J. Mater. Chem. A*, 2016, **4**, 5890.
- 49 L. Yang, S. Zhang, H. Chang, J. Zhang, H. Yao, Y. Yang, Z. Yun, W. Zhao and J. Hou, *J. Am. Chem. Soc.*, 2017, **139**, 1958.
- 50 H. Yao, Y. Cui, R. Yu, B. Gao, H. Zhang and J. Hou, *Angew. Chem. Int. Ed.*, 2017, **56**, 1.
- 51 F. Zhao, S. Dai, Y. Wu, Q. Zhang, J. Wang, L. Jiang, Q. Ling, Z. Wei, W. Ma, W. You, C. Wang and X. Zhan, *Adv. Mater.*, 2017, **29**, 1700144.
- 52 F. Yang, C. Li, W. Lai, A. Zhang, H. Huang and W. Li, *Mater. Chem. Front.*, 2017, **1**, 1389.
- 53 S. Dai, F. Zhao, Q. Zhang, T. K. Lau, T. Li, K. Liu, Q. Ling, C. Wang, X. Lu, W. You and X. Zhan, *J. Am. Chem. Soc.*, 2017, **139**, 1336.
- 54 W. Gao, Q. An, R. Ming, D. Xie, K. Wu, Z. Luo, Y. Zou, F. Zhang and C. Yang, *Adv. Funct. Mater.*, 2017, **27**, 1702194.
- 55 D. Xie, T. Liu, W. Gao, C. Zhong, L. Huo, Z. Luo, K. Wu, W. Xiong, F. Liu, Y. Sun and C. Yang, *Sol. RRL.*, 2017, **1**, 1700044.
- 56 H. Yao, L. Ye, J. Hou, B. Jang, G. Han, Y. Cui, G. M. Su, C. Wang, B. Gao, R. Yu, H. Zhang, Y. Yi, H. Y. Woo, H. Ade and J. Hou, *Adv. Mater.*, 2017, **29**, 1700254.
- 57 X. Bulliard, Y. W. Jin, G. H. Lee, S. Yun, D. S. Leem, T. Ro, K. B. Park, C. J. Heo, R. I. Satoh, T. Yagi, Y. S. Choi, S. J. Lim and S. Lee, *J. Mater. Chem. C*, 2016, **4**, 1117.
- 58 P. Solanke, S. Achelle, N. Cabon, O. Pytela, A. Barsella, B. Caro, R. L. Guen, J. Podlesný, M. Klikar and F. Bureš, *Dyes Pigm.*, 2016, **134**, 129.
- 59 S. Li, L. Ye, W. Zhao, S. Zhang, S. Mukherjee, H. Ade and J. Hou, *Adv. Mater.*, 2016, **28**, 9423.
- 60 C. Sun, Z. Wu, Z. Hu, J. Xiao, W. Zhao, L. I. Howa, Q. Y. Li, S. W. Tsang, Y. X. Xu, K. Zhang, H. L. Yip, J. Hou, F. Huang and Y. Cao, *Energy Environ. Sci.*, 2017, **10**, 1784.
- 61 Z. Wu, C. Sun, S. Dong, X. F. Jiang, S. Wu, H. Wu, H. L. Yip, F. Huang and Y. Cao, *J. Am. Chem. Soc.*, 2016, **138**, 2004.
- 62 P. K. Nayak, J. Bisquert and D. Cahen, *Adv. Mater.*, 2011, **23**, 2870.

Table of Contents Entry

Two new non-fullerene acceptors with expanded end-groups were developed, which present improved power conversion efficiency up to 9.0%.

